DRAFT
CMS Paper

The content of this note is intended for CMS internal use and distribution only

2015/10/08
Head Id: 297494
Archive Id: 301435M
Archive Date: 2015/07/21
Archive Tag: trunk

Search for Dark Matter in events with missing transverse momentum in association with jets or hadronically decaying vector bosons in pp collisions at $\sqrt{s} = 8$ TeV with the CMS detector.

The CMS Collaboration

Abstract

A search is presented for an excess of events with a large missing transverse momentum in association with a highly energetic jet in a data sample of proton-proton interactions at centre-of-mass energy of 8TeV. The data correspond to an integrated luminosity of 19.7 fb^{-1} collected by the CMS detector at the LHC. Additional sensitivity is achieved by tagging events consistent with the jet originating from a boosted hadronically decaying vector boson. The results are interpreted in the context of a set of simplified models for the production of dark matter.

1 Introduction

This paper describes a search for dark matter (DM) in events containing an energetic narrow or wide jet and an imbalance of transverse momentum ($E_{\mathrm{T}}^{\mathrm{miss}}$) in a dataset of pp collisions provided by the Large Hadron Collider (LHC) at a centre-of-mass energy of 8 TeV. The data were collected using the Compact Muon Solenoid (CMS) detector and correspond to an integrated luminosity of 19.7 fb^{-1}.

The existence of dark matter is one of the most compelling sources of evidence for physics beyond the Standard Model (SM) with a number of astrophysical observations suggesting an abundance of a non-baryonic form of matter in the universe. In many theories which extend the SM, the production of DM particles in high-energy hadron-hadron collisions, such as those produced at the Large Hadron Collider (LHC) is realised via a mediator which couples to both the SM and the DM particles. The canonical "monojet" search provides a model-independent means of exploring DM production at the LHC [1, 2] while related "mono-V" (V=W or Z boson) searches [3–7] target the associated production of DM with SM vector bosons, which can be enhanced in theories with non-universal DM couplings [8]. The interpretation of results from these and other DM searches at the Large Hadron Collider (LHC) have generally utilized effective field theories (EFT) that assume heavy mediators and DM production via contact interactions [9]. The results of this analysis are interpreted using the simplified DM models, [10–12], compatible with the recent recommendation of the LHC DM forum [13], which span a broad range of mediator and DM particle properties. This allows for a comparison in sensitivity with respect to direct detection experiments while retaining validity as a description of DM production across the entire kinematic region accessible at the LHC.

The search is the first at CMS to target the hadronic decay modes of the vector bosons in the mono-V channels. A multivariate V-tagging technique is employed to identify the individually resolved decay products of moderately boosted vector bosons. The exploration of mono-V production at high boost utilises recently developed techniques designed to exploit information available in the sub-structure of jets. The events are categorised according to the nature of the jets in the event and the signal extraction is performed by considering the $E_{\mathrm{T}}^{\mathrm{miss}}$ distribution in each event category. These two features provide improved sensitivity compared to the previous CMS monojet analysis [1].

This paper is structured as follows; Section 2 outlines the dark matter models explored as signal hypotheses and Section 3 provides a description of the physics object reconstruction and the event selection and categorisation used in the search. Section 4 describes the background modelling used for the signal extraction. The results of this analysis and interpretations of the results in the context of simplified models for DM production are presented in Section 5.

2 Signal Intepretations

The signal hypotheses targetted in this search are provided under a set of simplified mediator models. These models assume an additional particle, a fermionic dark matter candidate, and an additional interaction that forces the production of a dark matter. For generality, it is assumed that this additional interaction is mediated by a generic spin-0 or spin-1 particle. The interactions are characterised by four distinct Lagrangians, written for a Dirac-fermion dark matter particle χ as,

$$\mathcal{L}_{\text{scalar}} \supset -\frac{1}{2}m_{\text{MED}}^2 S^2 - g_{\text{DM}} S\,\bar{\chi}\chi - \sum_{q=b,t} g_{SM}^q S\,\bar{q}q - m_{\text{DM}}\bar{\chi}\chi\,, \tag{1}$$

$$\mathcal{L}_{\text{pseudo-scalar}} \supset -\frac{1}{2}m_{\text{MED}}^2 P^2 - i g_{\text{DM}} P\,\bar{\chi}\gamma^5\chi - \sum_{q=b,t} i g_{SM}^q P\,\bar{q}\gamma^5 q - m_{\text{DM}}\bar{\chi}\chi\,, \tag{2}$$

$$\mathcal{L}_{\text{vector}} \supset \frac{1}{2}m_{\text{MED}}^2 Z'_\mu Z'^\mu - g_{\text{DM}} Z'_\mu \bar{\chi}\gamma^\mu\chi - \sum_q g_{SM}^q Z'_\mu \bar{q}\gamma^\mu q - m_{\text{DM}}\bar{\chi}\chi\,, \tag{3}$$

$$\mathcal{L}_{\text{axial}} \supset \frac{1}{2}m_{\text{MED}}^2 Z''_\mu Z''^\mu - g_{\text{DM}} Z''_\mu \bar{\chi}\gamma^\mu\gamma^5\chi - \sum_q g_{SM}^q Z''_\mu \bar{q}\gamma^\mu\gamma^5 q - m_{\text{DM}}\bar{\chi}\chi \tag{4}$$

assuming pure scalar, psuedoscalar, axial-vector and vector mediated interactions denoted by S, P, Z' and Z'' mediators respectively. The couplings g_{DM} and g_{SM} denotes the coupling of the mediator to the dark matter particle and to standard model particles respectively. The choice of this split in the Lagrangian is to parallel the existing separation with direct detection, into spin-dependent and spin-independent interactions. Here, spin-independent can refer to either vector or scalar mediated interactions, between which direct detection makes no distinction, while spin-dependent interactions refer to axial-vector mediated processes. Pseudoscalar interactions are velocity suppressed in DM-nucleon interactions and thus limited sensitivity from the direct detection experiments is expected [14]. An extension to the scalar and pseudoscalar can be performed by allowing the (pseudo-)scalar interactions to undergo electroweak symmetry breaking (EWSB) in an analogous way to the Higgs mechanism [15–21]. Scalar and pseudoscalar models where EWSB is not present are denoted herein as *fermionic* dark matter production.

In collider experiments, the production of dark matter in spin-0 mediated interactions is predominantly through gluon-fusion via a top-quark loop. When EWSB is present in the model, mono-V signatures are produced through the well known higgs-strahlung process. For the spin-1 signatures, dark matter is produced in an analogous way to Z boson production through quark initiated processes. The mono-V or monojet signatures follow from the presence of a radiated V-boson or jet in the initial state. In all models, the coupling of the mediator to standard model coupling is taken as unity ($g_{SM} = 1$) along with the dark matter coupling ($g_{DM} = 1$). For the (pseudo-)scalar models, this denotes a Yukawa coupling to standard model particles. For all models considered, the width is fixed under the minimum width constraint [22].

In order to model the expected contribution from these signals, Monte Carlo (MC) events are generated using MCFM [23] for the monojet final state, and JHUGen [24] for the vector boson final state. All signal models are generated at leading order, showered with Pythia6 and passed through a simulation of the CMS detector using Geant4 [25]. For scalar and pseudoscalar mediated DM production, the finite top mass is taken into account.

3 Event Selection and Categorization

Signal events are selected on the basis of large values of $E_{\text{T}}^{\text{miss}}$ and one or more high-p_{T} jet(s), explicitly vetoing isolated leptons and photons. Events are reconstructed with the CMS detector, following the standard CMS reconstruction [26].

The data used for this analysis are collected using either of two triggers designed to record events containing contain a large $E_{\text{T}}^{\text{miss}}$. The first requires a $E_{\text{T}}^{\text{miss}}$ of greater than 120 GeV, calculated only using information from the calorimeter, while the second requires an $E_{\text{T}}^{\text{miss}}$ greater

than 95 GeV or 105 GeV, depending on the data-taking period, calculated using the online version of the particle flow (PF) reconstruction algorithm [27] as well as a reconstructed well identified jet with $p_{\mathrm{T}} > 80$ GeV and $|\eta| < 2.6$. The threshold on the $E_{\mathrm{T}}^{\mathrm{miss}}$ for the selection of the events is set at 200 GeV in order to maintain a trigger efficiency greater than 99% with respect to the full event selection.

Jets are reconstructed from the clustering of PF objects using either the anti-k_{T} algorithm [28] with 0.5 (ak5 jet) as the distance parameter, or the Cambridge/Aachen algorithm [29] with 0.8 distance parameter (ca8). The leading jet is further required to be well identified, using a standard set of identification criteria [30]. The jets are corrected for pileup on the basis of the event energy density and proportionally to their area. Data-driven calibrations are then applied to correct the absolute scale of the jet energy [30].

The $E_{\mathrm{T}}^{\mathrm{miss}}$ is calculated as the magnitude of the negative vector sum of the transverse momenta of all final state particles, which are reconstructed using the particle-flow (PF) algorithm [27]. Events with a large mis-reconstructed offline $E_{\mathrm{T}}^{\mathrm{miss}}$ are removed by applying quality filters. The angle between the $E_{\mathrm{T}}^{\mathrm{miss}}$ and the leading jet is required to be larger than 2 to reduce the contribution from multijet QCD events. Finally, events are vetoed if they contain at least one well-identified and isolated electron, photon or muon with $p_T > 10$ GeV, or a tau with $p_T > 15$ GeV.

Selected events are classified into three event categories, based on the topology of the jets, in order to distinguish between initial or final state radiation of gluons or quarks and jets arising from hadronic vector boson decays. The categories are first scrutinized for the presence of an unresolved vector boson (boosted category), subsequently for a resolved vector boson (resolved category), and finally the remaining events are collected into the monojet category.

If the vector boson decays hadronically and has sufficiently high transverse momentum, both its hadronic decay products are captured by a single reconstructed "fat"-jet. Events in the boosted vector boson category are required to have a reconstructed ca8 jet with $p_{\mathrm{T}} > 200$ GeV and $E_{\mathrm{T}}^{\mathrm{miss}} > 250$ GeV. Further cuts are applied to improve the vector boson jet purity by cutting on the variable "N-subjettiness" for 2-pronged jets (τ_2/τ_1 defined in [31, 32]) and the pruned jet mass [33]. The τ_2/τ_1 ratio is required to smaller than 0.5 and the pruned jet mass, m_{prune}, is selected to be close to both the W and Z boson masses, namely to satisfy $60 < m_{\mathrm{prune}} < 110$ GeV. Events which contain additional jets close to the ca8 jet, but no closer than $\Delta R < 0.5$, are selected to include the frequent cases in which initial state radiation yields additional jets. If an ak5 jet with $p_T > 30$ and $|\eta| < 2.5$ is reconstructed, and the opening angle between it and the ca8 jet, $\Delta\phi(\mathrm{ak5}, \mathrm{ca8})$, is smaller than 2, the event is selected. Events with more than one ak5 jets with $p_T > 30$ GeV and $|\eta| < 2.5$, reconstructed at $\Delta R > 0.5$ with respect to the ca8 jet are rejected.

In cases where the electroweak boson has insufficient transverse momentum for its hadronic decay to be fully contained in a single reconstructed fat-jet, a selection that looks for decays into a pair of ak5 jets is applied to recover the event. The selection requires that each jet has $p_T > 30$ GeV and $|\eta| < 2.5$ and that the dijet has a mass between 60 GeV and 110 GeV, consistent with originating from a W or Z boson. To further reduce the combinatorial background, a multivariate V-tagger is applied. The inputs to this resolved V-tagger are the values from each jet of likelihood-based discriminator variable which distinguishes quark-initiated jets from gluon-initiated jets [34], the jet pull angle [35] and the mass drop variable [36]. In events where multiple dijet pairs are found, the pair with the highest V-tagger value is taken as the candidate. To reduce contamination from top backgrounds, the event is rejected if it contains a b-tagged jet, defined using the CSV medium definition [37]. Finally, the events are required to have

$E_{\mathrm{T}}^{\mathrm{miss}} > 250$ GeV.

The events that do not qualify for either of the two V-tagged categories are tested for the presence of a single jet originating from quark or gluon radiation. For the monojet category, at least one ak5 jet within $|\eta| < 2.0$ with p_{T} greater than 150 GeV and a $E_{\mathrm{T}}^{\mathrm{miss}}$ greater than 200 GeV is required. As in the boosted category, events with a second ak5 jet close to the leading one ($\Delta\phi(j_1, j_2) < 2$) with $p_T > 30$ GeV and $|\eta| < 2.5$ are selected to allow the frequent cases where initial state radiation yields two jets. Events with three or more ak5 jets with $p_T > 30$ GeV and $|\eta| < 2.5$ are rejected.

To model the expectation from SM backgrounds, simulated samples are produced for the Z+jets, W+jets, $t\bar{t}$, single-top, and QCD multi-jet processes using Madgraph [38] interfaced with Pythia6 [39] for hadronization and fragmentation, where jets from the matrix element are matched to the parton shower following the MLM matching prescription [40]. Additionally a single-top background sample, produced with POWHEG [41], a set of diboson samples, produced directly with Pythia6, are added. All are processed using Geant4 [25], providing a full simulation of the CMS detector. The MC samples are corrected to account for the distribution of the number of additional (pileup or PU) interactions observed in 2012 dataset. Both signal and background samples are additionally corrected to account for the mis-modelling of hadronic recoil in simulation following the procedure described in [42].

Figure 1 shows the $E_{\mathrm{T}}^{\mathrm{miss}}$ and leading jet p_T distributions in data and simulation after selection for all three event classes combined. The backgrounds are normalized to 19.7 fb^{-1} and the expected distribution for vector mediated DM production assuming a DM mass of 10 GeV and mediator mass of 1 GeV is shown. The discrepancy between the data and simulation is a result of both mis-modelling of the detector resolution and an imperfect theoretical description of the kinematics of the W/Z+jet processes. Both effects are corrected for in this analysis using a data-driven approach described in the following section.

4 Signal Extraction

The presence of DM production will be observable as an excess of events with respect to the expectations for the SM backgrounds in a region at high missing transverse energy. Significant improvements in terms of sensitivity can be expected if several bins in $E_{\mathrm{T}}^{\mathrm{miss}}$ are considered simultaneously. A binned likelihood fit is performed in the range 250 GeV to 1000 GeV (or 200 GeV to 1000 GeV for the monojet category), where the binning is chosen to ensure each corresponding bin of the control regions is populated. The width of the highest $E_{\mathrm{T}}^{\mathrm{miss}}$ bin allows for ease of comparison to the previous CMS search [1].

Data from three control regions, the dimuon and photon control regions, and the single-muon control region, are used to determine the contributions from $Z(\nu\nu) + \text{jets}$ and $W(l\nu) + \text{jets}$ respectively. The events in the control regions are divided into the three categories, using the same selection criteria as described in Section 3. In the dimuon, single-muon and photon control regions, the dimuon pair, single-muon or the photon's momentum are removed and the $E_{\mathrm{T}}^{\mathrm{miss}}$ is recalculated yielding a distribution of fake $E_{\mathrm{T}}^{\mathrm{miss}}$. The distribution of fake $E_{\mathrm{T}}^{\mathrm{miss}}$ in data in the control regions is used to derive the expectation from the Z+jets and W+jets backgrounds in the signal region.

As the decay branching ratio of $Z \to \mu^+\mu^-$ is approximately 6 times smaller than that to neutrinos, the resulting statistical uncertainty on the $Z(\nu\nu) + \text{jets}$ template becomes a dominant systematic uncertainty at large values of $E_{\mathrm{T}}^{\mathrm{miss}}$. A complementary approach is to additionally

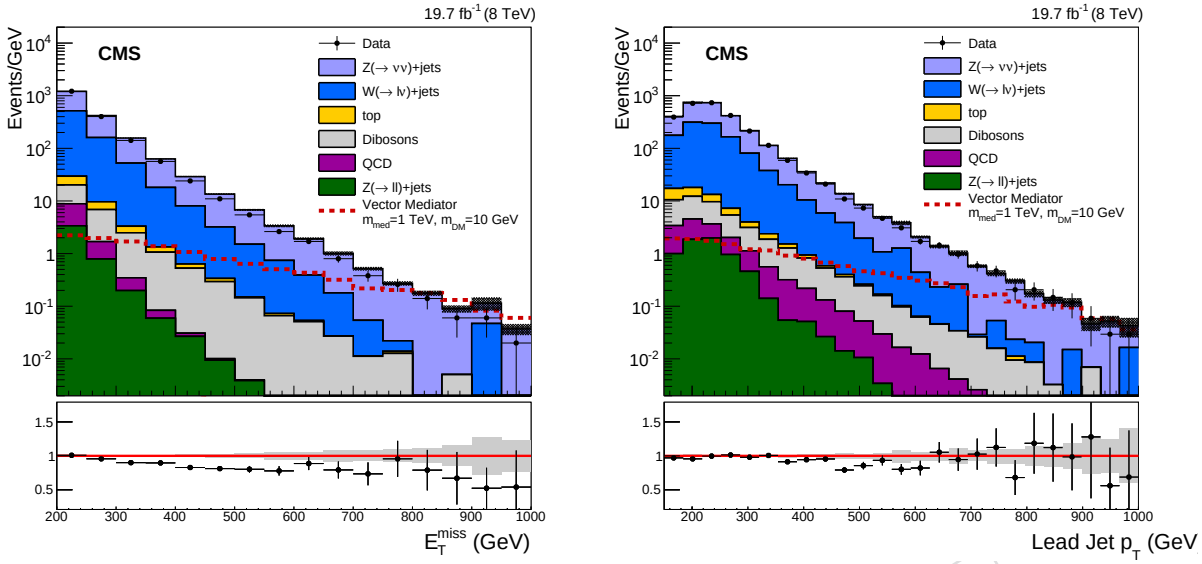

(a) (b)

Figure 1: Distributions of $E_{\mathrm{T}}^{\mathrm{miss}}$ (a) and leading jet p_T (b) in simulated events and data after the signal selection for all three event categories combined. The dashed red line shows the expected distribution assuming vector mediated DM production with $m_{DM} = 10$ GeV and $m_{MED} = 1$ TeV. The gray band in the ratio panels indicate the statistical uncertainty from the limited number of background MC events.

use events in data that have a high-p_T photon recoiling against jets to further constrain the $Z(\nu\nu)+$jets background template [43] as the production cross-section of $\gamma+$jets is roughly 3 times that of the $Z(\nu\nu)+$jets resulting in a smaller statistical uncertainty on the predicted background.

The $E_{\mathrm{T}}^{\mathrm{miss}}$ spectra of the V+jets backgrounds is determined through the use of a likelihood fit, simultaneously across all bins in the three control regions. The expected number of events N_i in a given bin i of fake $E_{\mathrm{T}}^{\mathrm{miss}}$, for a particular event category, is given by, $N_i^{Z_{\mu\mu}|\gamma} = \dfrac{\mu_i^{Z\to\nu\nu}}{R_i^{Z|\gamma}}$, for the dimuon and photon control regions and $N_i^{W} = \dfrac{\mu_i^{W\to l\nu}}{R_i^{W}}$, for the single-muon control region. The parameters $\boldsymbol{\mu}^{Z\to\nu\nu}$ and $\boldsymbol{\mu}^{W\to l\nu}$ are the free parameters of the likelihood representing the yields of $Z(\nu\nu)+$jets and $W(l\nu)+$jets in each bin of the signal region. The likelihood function for a particular category, c, is given as,

$$\begin{aligned}\mathcal{L}_{\mathrm{c}}(\boldsymbol{\mu}^{\mathrm{c},Z\to\nu\nu},\boldsymbol{\mu}^{\mathrm{c},W\to l\nu},\boldsymbol{\theta},\boldsymbol{\phi}) = &\prod_i \mathrm{Poisson}\left(d_i^{\mathrm{c},\gamma}|B_i^{\mathrm{c},\gamma}(\boldsymbol{\phi}) + \frac{\mu_i^{\mathrm{c},Z\to\nu\nu}}{R_i^{\mathrm{c},\gamma}(\boldsymbol{\theta})}\right)\\ &\times\prod_i \mathrm{Poisson}\left(d_i^{\mathrm{c},Z}|B_i^{\mathrm{c},Z}(\boldsymbol{\phi}) + \frac{\mu_i^{\mathrm{c},Z\to\nu\nu}}{R_i^{\mathrm{c},Z}(\boldsymbol{\theta})}\right)\\ &\times\prod_i \mathrm{Poisson}\left(d_i^{\mathrm{c},W}|B_i^{\mathrm{c},W}(\boldsymbol{\phi}) + \frac{\mu_i^{\mathrm{c},W\to l\nu}}{R_i^{\mathrm{c},W}(\boldsymbol{\theta})}\right),\end{aligned} \tag{5}$$

where $d_i^{c,\gamma/Z/W}$ are the observed number of events in each bin of the photon, dimuon and single-muon control regions. The expected contributions from background processes in the dimuon, single-muon and photon control regions are denoted B^Z, B^W and B^γ in equation **??** respectively.

The transfer factors R_i^Z account for the ratio of $BR(Z \to \nu\nu)/BR(Z \to \mu^+\mu^-)$ and the muon efficiency times acceptance in the dimuon control region, while R_i^γ account for the ratio of differential cross-sections between the Z+jet and photon+jet processes and the efficiency times acceptance of the photon selection for the photon plus jet control region.The differential boson p_T cross-sections of photon and Z production are first corrected using NLO k-factors derived by comparing their p_T distributions in events generated at single parton level with Madgraph5_aMC@NLO [38], and subsequently showered, to the distributions produced at leading order before deriving the transfer factors.

Systematic uncertainties are modelled as constrained nuisance parameters, $\boldsymbol{\theta}$, which allow for variation of the transfer factors, $R^{\gamma/Z/W}$, in the fit and are treated as fully correlated between event categories. These include theoretical uncertainties on the photon to Z differential cross-section ratio from renormalization and factorization scale uncertainties. Electroweak corrections to the ratio are not accounted for in the simulation. The full correction is also taken as an uncertainty on the ratio, which is of the order of 15% when the boson (Z or γ) p_{T} is at the TeV scale [44]. A conservative choice is made in assuming this uncertainty to be uncorrelated across bins of $E_{\mathrm{T}}^{\mathrm{miss}}$. Additionally, the uncertainty in the muon selection efficiency, photon selection efficiency, and photon purity are included and fully correlated across the event categories and control regions, where relevant. A systematic uncertainty of 10% is included for the background normalization [45] and correlated between the single-muon and dimuon control regions.

The remaining backgrounds are expected to be much smaller than those from V+jets and are estimated directly from the simulation. Shape and normalization systematic uncertainties from the recoil corrections applied to these backgrounds are included to account for the uncertainty in the energy scale and resolution of jets. Additionally, a systematic uncertainty of 4% is included for the top backgrounds due to the uncertainty of the b-tagging efficiency for the b-jet veto in the resolved category. Systematic uncertainties of 7%, 10% and 50% are included for the top, diboson and QCD backgrounds respectively to account for the uncertainty in their production cross-sections. Finally, a systematic uncertainty of 2.6% in the luminosity measurement [46] is included for all of the MC derived backgrounds.

5 Results

A simultaneous fit to the signal region across the three event categories, allowing for sytematic uncertainty variations of the background expectations, is performed. The corresponding comparisons between data and background in the $E_{\mathrm{T}}^{\mathrm{miss}}$ distributions, for each of the three categories, after this fit are shown in Figure 2. Agreement between the expected SM backgrounds and data is observed at the percent level across the three categories. The largest single-bin local significance across the three categories, is 1.9σ and corresponds to the excess seen in the last $E_{\mathrm{T}}^{\mathrm{miss}}$ bin of the monojet category.

Exclusion limits are set for a these models using the CLs method [47] with a profile likelihood ratio as the test-statistic in which systematic uncertainties are modelled as nuisance parameters. For each signal hypothesis tested, upper limits are placed on the ratio of the signal cross-section to the predicted cross-section, denoted as $\mu = \sigma/\sigma_{TH}$. Limits are presented in terms of excluded

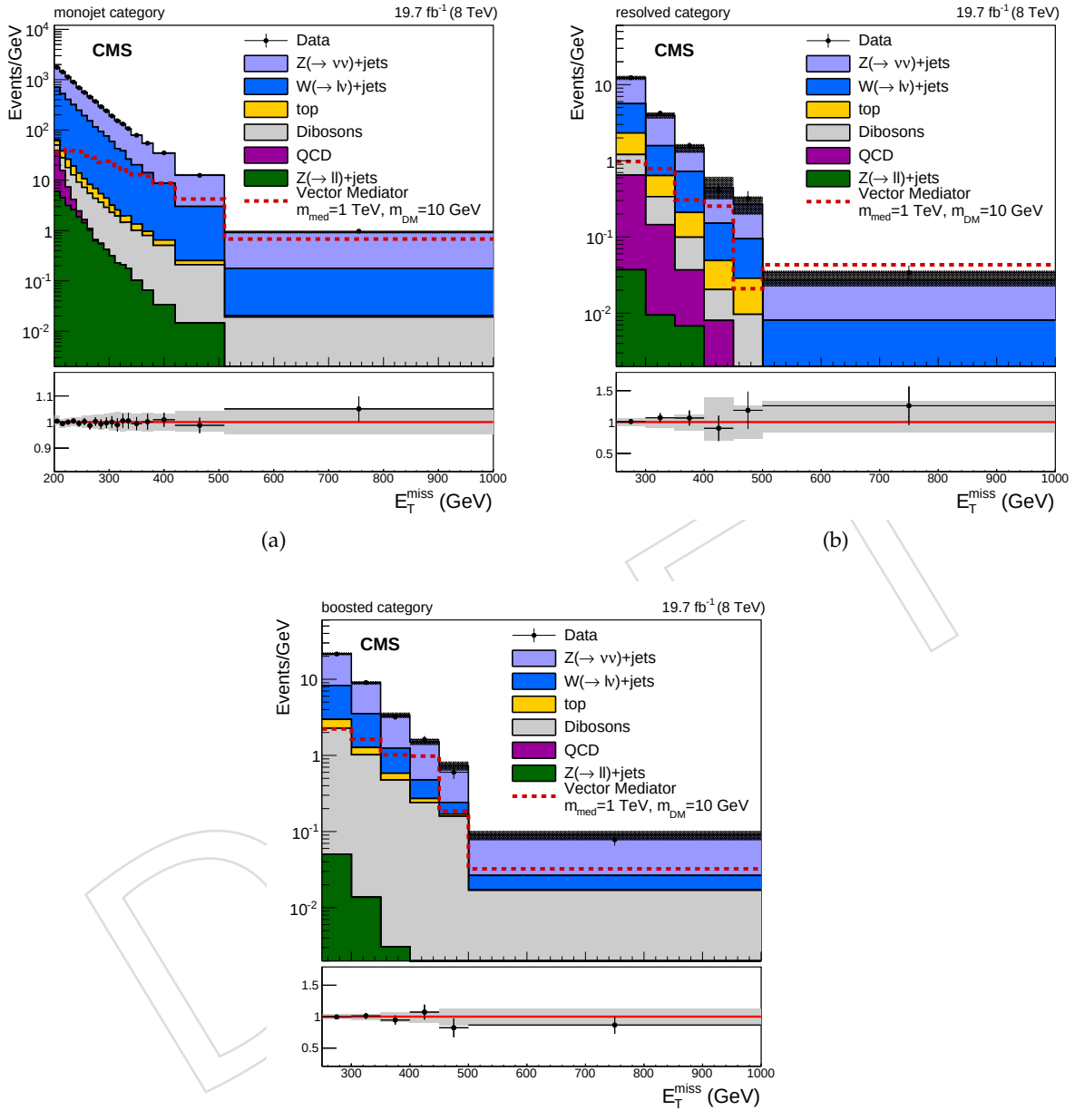

(a) (b)

(c)

Figure 2: Post-fit distributions of $E_{\mathrm{T}}^{\mathrm{miss}}$ expected from SM backgrounds and observed in data in the signal region. The expected distributions are evaluated after fitting to the observed data simultaneously across the monojet (a), resolved (b) and boosted (c) categories. The gray bands indicate the post-fit uncertainty on the background, assuming no signal. The expected distribution assuming vector mediated DM production is shown for a DM mass of 10 GeV and a mediator mass of 1 TeV.

regions in the $m_{\mathrm{MED}} - m_{\mathrm{DM}}$ plane, assuming the four different mediators, by determining the points for which $\mu \geq 1$ is excluded at 90% CL or more. Experimental systematic uncertainties, including jet and $E_{\mathrm{T}}^{\mathrm{miss}}$ response and resolution, are included on the signal model as nuisance parameters, while the theoretical systematic uncertainties on the inclusive cross-section (20% and 30% for the vector and axial-vector, and scalar and pseudoscalar models respectively) due to QCD scale and PDF uncertainties are instead added as additional contours to the exclusion limits. These uncertainties are chosen to be conservative across the full range in mediator mass.

To compare direct detection experiments with collider experiments, the direct detection bounds can be interpreted under the Lagrangians given in Equation 1. The limits obtained in the simplified models are obtained using the standard approaches to compute t-channel scattering [12, 48–50]. For the vector and scalar mediator models, the limits are compared with the measurements by LUX [51–53] which currently provides the strongest bounds for $m_{\mathrm{DM}} \gtrsim 6$ GeV. For axial-vector couplings, the limits are compared with the combined bounds of DM-proton-scattering limits of PICASSO [54], COUPP [55] and SIMPLE [56], while for the pseudoscalar case, the comparison is made with constraints from FermiLAT [57, 58]. For pseudoscalar interactions, direct detection bounds are strongly velocity suppressed. The most appropriate comparison is therefore to the most sensitive bounds from indirect detection from FermiLAT. These limits apply to the scenario in which dark matter is annihilated in the center of a galaxy producing a γ ray signature. The results are also compared, for all four types of mediators, to constraints obtained from the observed cosmological relic density of DM as determined from measurements of the cosmic microwave background by the WMAP and Planck experiments [59, 60]. The expected DM abundance is estimated, separately for each model, using a thermal freeze-out mechanism implemented in MadDM [61], and compared to the observed cold DM density $\Omega_c * h^2 = 0.12$ [62]. It is assumed that the simplified model hypothesised provides the only relevant BSM dynamics for DM interactions.

Figure 3 shows the 90% CL exclusions for the vector, axial-vector, scalar and pseudoscalar mediator models. The 90% confidence level upper limit on the ratio of excluded cross-section to the predicted cross-section (μ_{up}), when assuming the mediator only couples to fermions, is shown by the blue color scale. These limits are calculated under the assumption that only the initial state partons and the DM particle contribute to the width of the mediator. For all models, the width is fixed under the minimum width constraint [9, 10, 13, 63]. Under the vector mediator model, the direct detection bounds dominate across most of the plane, while for the axial-vector, there is good complementarity between the direct detection limits and those from this analysis. Limits in the scalar mediator scenario are much weaker than those from direct detection for small dark-matter masses. Additional sensitivity is gained for larger mediator masses in this scenario above 350 GeV due to the rise in cross-section of the gluon fusion loop process above the $t\bar{t}$ threshold. In the pseudoscalar mediator scenario, the limits from this analysis exceed the reach in m_{MED} than those from FermiLAT.from this analysis dominate over the whole region.

Figures 4a, 4b and 4c show the same exclusion contours, this time translated into the plane of $m_{\mathrm{DM}} - \sigma_{\mathrm{SI/SD}}$, where $\sigma_{\mathrm{SI/SD}}$ are the spin-independent/dependant (vector and scalar/axial-vector) DM-nucleon scattering cross-sections. These representations allow for a more direct comparison with limits from the direct-detection experiments which typically set upper limits on these cross-sections [64, 65]. It should be noted that the limits set from this analysis are however only valid under the simplified model considered, and in particular assuming $g_{\mathrm{DM}} = g_{\mathrm{SM}} = 1$. For the scalar model, it is assumed that only heavy quarks (top and bottom) contribute. Such a choice limits the sensitivity for direct detection, however it allows for direct comparison between collider and direct detection without an additional assumption on the

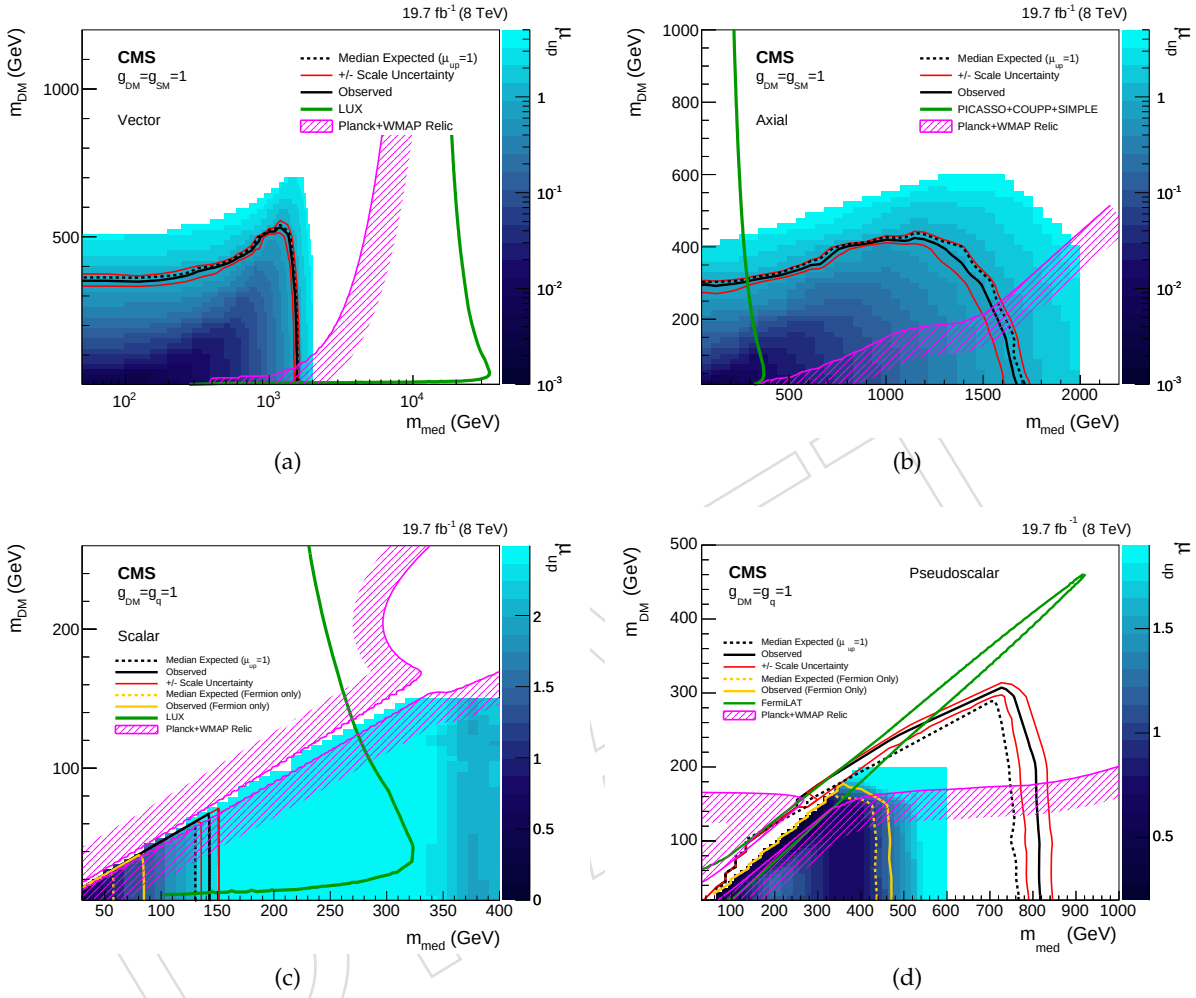

Figure 3: 90% CL Exclusion contours in the $m_{\text{med}} - m_{\text{DM}}$ plane assuming a vector (a), axial-vector (b), scalar (c), or pseudoscalar (d) mediator. The blue scale shows the 90% CL upper limit on the signal strength assuming the mediator only couples to fermions. For the scalar and pseudoscalar mediators, the exclusion contour assuming coupling only to fermions is explicitly shown in the orange line. The white region shows model points which were not tested when assuming coupling only to fermions and are not expected to be excluded by this analysis under this assumption. The excluded region is to the bottom-left of the contours shown in all cases except for that from the relic density as indicated by the shading. In all of the mediator models, a minimum width is assumed.

light quark couplings [65]. For the vector and scalar mediator models, direct-detection limits are stronger than those obtained in this analysis except in the scenario where the dark matter mass is less than around 6 GeV while for the axial-vector mediator model, the limits obtained in this analysis dominate up to around $m_{\mathrm{DM}} = 300$ GeV.

The excess observed in FermiLAT data has led to speculations that dark matter annihilation is mediated by a light pseudoscalar [66]. The production mechanism for these γ rays can be interpreted under dark matter annihilation to b-quarks allowing for direct comparison limits from this analysis [22, 67, 68]. Figure 4d shows the exclusion contours assuming pseudoscalar mediation in the plane of DM pair annihilation cross-section versus m_{DM}. It is assumed that only heavy quarks (top and bottom quarks) contribute in the production of the mediator while for the interpretation of the limits in the annihilation cross-section, it is assumed that the mediator only decays to b-quark pairs. Such a choice limits the sensitivity for direct detection, however it allows for direct comparison between collider and direct detection without an additional assumptions on the light quark couplings [65]. As with all interpretations, the DM particle is assumed to be a Dirac fermion. The 68% CL preferred regions in this plane assuming the annihilation of DM pairs to light-quarks (qq), tau or bottom pairs, using data from FermiLAT, are shown as solid colour regions. Under the simplified model used, all of these regions are excluded by this analysis.

6 Summary

A search has been presented for an excess of events with a high energy jet in association with a large missing transverse momentum in a data sample of proton-proton interactions at centre-of-mass energy of 8 TeV. The data correspond to an integrated luminosity of 19.7 fb^{-1} collected by the CMS detector at the LHC. Sensitivity to mono-V models is achieved by tagging events consistent with the jet originating from a hadronically decaying vector boson. No significant deviation from the expectation from SM backgrounds is observed in the $E_{\mathrm{T}}^{\mathrm{miss}}$ distributions. The search is interpreted in terms of DM production to place constraints on the parameter space of the simplified models considered.

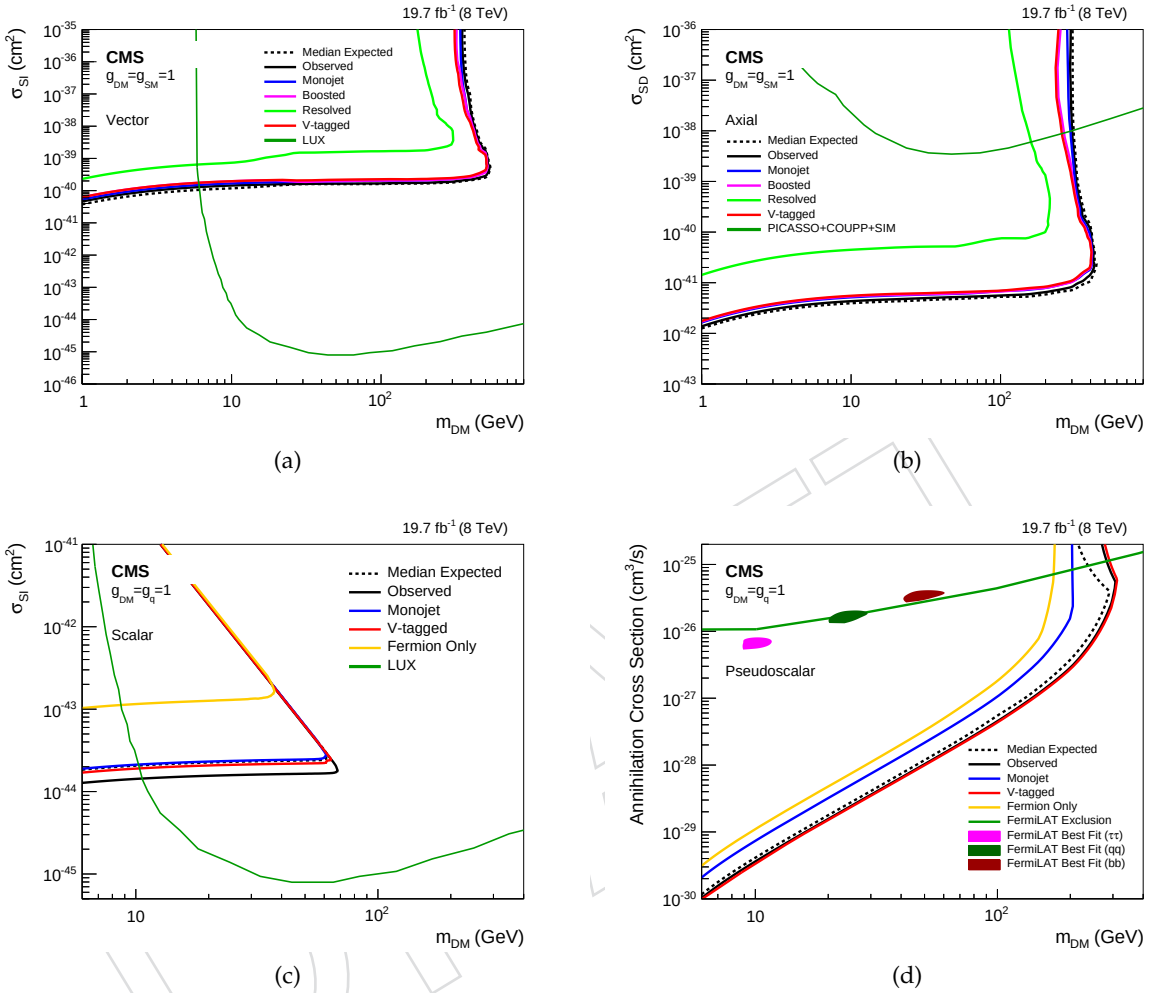

Figure 4: 90% CL Exclusion contours in the $m_{\mathrm{DM}} - \sigma_{\mathrm{DM}}$ plane assuming a vector (a), axial-vector (b), scalar (c), or pseudoscalar (d) mediator. For the scalar and pseudoscalar case, the orange line shows the exclusion contours assuming the mediator only couples to fermions. The excluded region in all plots is to the top left of the contours shown. In the vector and axial-vector scenarios, limits are shown independently for monojet, boosted and resolved categories. The partial combination of the "V-tagged" categories (resolved and boosted) categories is shown for which the boosted category provides the dominant contribution. In all of the mediator models, a minimum width is assumed. For the pseudoscalar, 68% CL preferred regions, using data from FermiLAT, for DM annihilation to light-quarks (qq), tau pairs ($\tau\tau$) and bottom-quark pairs (bb) are shown by the solid green, pink and brown coloured regions respectively.

References

[1] CMS Collaboration, "Search for dark matter, extra dimensions, and unparticles in monojet events in protonproton collisions at $\sqrt{s} = 8$ TeV", *Eur.Phys.J.* **C75** (2015), no. 5, 235, doi:10.1140/epjc/s10052-015-3451-4, arXiv:1408.3583.

[2] ATLAS Collaboration, "Search for new phenomena in final states with an energetic jet and large missing transverse momentum in pp collisions at $\sqrt{s} = 8$ TeV with the ATLAS detector", arXiv:1502.01518.

[3] CMS Collaboration, "Search for physics beyond the standard model in final states with a lepton and missing transverse energy in proton-proton collisions at sqrt(s) = 8 TeV", *Phys.Rev.* **D91** (2015), no. 9, 092005, doi:10.1103/PhysRevD.91.092005, arXiv:1408.2745.

[4] CMS Collaboration, "Search for invisible decays of Higgs bosons in the vector boson fusion and associated ZH production modes", *Eur.Phys.J.* **C74** (2014), no. 8, 2980, arXiv:1404.1344.

[5] ATLAS Collaboration, "Search for dark matter in events with a Z boson and missing transverse momentum in pp collisions at $\sqrt{s}$=8 TeV with the ATLAS detector", *Phys. Rev.* **D90** (2014), no. 1, 012004, doi:10.1103/PhysRevD.90.012004, arXiv:1404.0051.

[6] ATLAS Collaboration, "Search for dark matter in events with a hadronically decaying W or Z boson and missing transverse momentum in pp collisions at $\sqrt{s} = 8$ TeV with the ATLAS detector", *Phys. Rev. Lett.* **112** (2014), no. 4, 041802, doi:10.1103/PhysRevLett.112.041802, arXiv:1309.4017.

[7] ATLAS Collaboration, "Search for new particles in events with one lepton and missing transverse momentum in pp collisions at $\sqrt{s}$ = 8 TeV with the ATLAS detector", *JHEP* **09** (2014) 037, doi:10.1007/JHEP09(2014)037, arXiv:1407.7494.

[8] Feng, J. *et al.*, "Isospin-Violating Dark Matter", (2011). arXiv:1102.4331.

[9] P. J. Fox, R. Harnik, J. Kopp, and Y. Tsai, "Missing Energy Signatures of Dark Matter at the LHC", *Phys.Rev.* **D85** (2012) 056011, arXiv:1109.4398.

[10] Busoni, G. *et al.*, "On the Validity of the Effective Field Theory for Dark Matter Searches at the LHC", *Phys. Lett. B* **728C** (2014) 412–421.

[11] O. Buchmueller, M. J. Dolan, and C. McCabe, "Beyond Effective Field Theory for Dark Matter Searches at the LHC", *JHEP* **1401** (2014) 025, arXiv:1308.6799.

[12] O. Buchmueller, M. J. Dolan, S. A. Malik, and C. McCabe, "Characterising dark matter searches at colliders and direct detection experiments: Vector mediators", *JHEP* **01** (2015) 037, doi:10.1007/JHEP01(2015)037, arXiv:1407.8257.

[13] D. Abercrombie et al., "Dark Matter Benchmark Models for Early LHC Run-2 Searches: Report of the ATLAS/CMS Dark Matter Forum", arXiv:1507.00966.

[14] U. Haisch, F. Kahlhoefer, and J. Unwin, "The impact of heavy-quark loops on LHC dark matter searches", *JHEP* **07** (2013) 125, doi:10.1007/JHEP07(2013)125, arXiv:1208.4605.

[15] V. V. Khoze, G. Ro, and M. Spannowsky, "Spectroscopy of Scalar Mediators to Dark Matter at the LHC and at 100 TeV", arXiv:1505.03019.

[16] T. Hambye and A. Strumia, "Dynamical generation of the weak and Dark Matter scale", *Phys. Rev.* **D88** (2013) 055022, doi:10.1103/PhysRevD.88.055022, arXiv:1306.2329.

[17] V. V. Khoze, C. McCabe, and G. Ro, "Higgs vacuum stability from the dark matter portal", *JHEP* **08** (2014) 026, doi:10.1007/JHEP08(2014)026, arXiv:1403.4953.

[18] V. V. Khoze and G. Ro, "Dark matter monopoles, vectors and photons", *JHEP* **10** (2014) 61, doi:10.1007/JHEP10(2014)061, arXiv:1406.2291.

[19] W. Altmannshofer et al., "Light Dark Matter, Naturalness, and the Radiative Origin of the Electroweak Scale", *JHEP* **01** (2015) 032, doi:10.1007/JHEP01(2015)032, arXiv:1408.3429.

[20] C. D. Carone and R. Ramos, "Classical scale-invariance, the electroweak scale and vector dark matter", *Phys. Rev.* **D88** (2013) 055020, doi:10.1103/PhysRevD.88.055020, arXiv:1307.8428.

[21] M. Heikinheimo et al., "Physical Naturalness and Dynamical Breaking of Classical Scale Invariance", *Mod. Phys. Lett.* **A29** (2014) 1450077, doi:10.1142/S0217732314500771, arXiv:1304.7006.

[22] P. Harris, V. V. Khoze, M. Spannowsky, and C. Williams, "Constraining Dark Sectors at Colliders: Beyond the Effective Theory Approach", *Phys.Rev.* **D91** (2015), no. 5, 055009, doi:10.1103/PhysRevD.91.055009, arXiv:1411.0535.

[23] J. M. Campbell and R. K. Ellis, "MCFM for the Tevatron and the LHC", *Nucl. Phys. Proc. Suppl.* **205-206** (2010) 10–15.

[24] I. Anderson et al., "Constraining anomalous HVV interactions at proton and lepton colliders", *Phys.Rev.* **D89** (2014), no. 3, 035007, arXiv:1309.4819.

[25] S. Agostinelli, J. Allison, K. Amako et al., "Geant4 - a simulation toolkit", *Nuclear Instruments and Methods in Physics Research Section A: Accelerators, Spectrometers, Detectors and Associated Equipment* **506** (2003), no. 3, 250 – 303.

[26] CMS Collaboration, "The CMS experiment at the CERN LHC", *JINST* **3** (2008) S08004.

[27] CMS Collaboration, "Particle-Flow Event Reconstruction in CMS and Performance for Jets, Taus, and MET", Technical Report CMS-PAS-PFT-09-001, CERN, 2009. Geneva, Apr, 2009.

[28] M. Cacciari, G. P. Salam, and G. Soyez, "The Anti-k(t) jet clustering algorithm", **04** (2008) 063, doi:10.

[29] CMS Collaboration, "A Cambridge-Aachen (C-A) based Jet Algorithm for boosted top-jet tagging", Technical Report CMS-PAS-JME-09-001, CERN, 2009. Geneva, Jul, 2009.

[30] CMS Collaboration, "Determination of jet energy calibration and transverse momentum resolution in CMS", *Journal of Instrumentation* **6** (November, 2011) 11002, doi:10.1088/1748-0221/6/11/P11002, arXiv:1107.4277.

[31] J. Thaler and K. Van Tilburg, "Identifying boosted objects with N-subjettiness", *JHEP* **03** (2011) 015, arXiv:1011.2268.

[32] J. Thaler and K. Van Tilburg, "Maximizing boosted top identification by minimizing N-subjettiness", *JHEP* **02** (2012) 093, arXiv:1108.2701.

[33] S. D. Ellis, C. K. Vermilion, and J. R. Walsh, "Recombination Algorithms and Jet Substructure: Pruning as a Tool for Heavy Particle Searches", *Phys.Rev.* **D81** (2010) 094023, arXiv:0912.0033.

[34] CMS Collaboration, "V Tagging Observables and Correlations", CMS Physics Analysis Summary CMS-PAS-JME-14-002, 2014.

[35] J. Gallicchio and M. D. Schwartz, "Seeing in Color: Jet Superstructure", *Phys.Rev.Lett.* **105** (2010) 022001, arXiv:1001.5027.

[36] E. Izaguirre, B. Shuve, and I. Yavin, "Improving Identification of Dijet Resonances at Hadron Colliders", *Phys.Rev.Lett.* **114** (2015), no. 4, 041802, doi:10.1103/PhysRevLett.114.041802, arXiv:1407.7037.

[37] CMS Collaboration, "Identification of b-quark jets with the CMS experiment", *JINST* **8** (2013) P04013, arXiv:1211.4462.

[38] J. Alwall et al., "The automated computation of tree-level and next-to-leading order differential cross sections, and their matching to parton shower simulations", *JHEP* **1407** (2014) 079, arXiv:1405.0301.

[39] T. Sjöstrand, S. Mrenna, and P. Skands, "PYTHIA 6.4 physics and manual", *JHEP* **05** (2006) 026, arXiv:hep-ph/0603175.

[40] M. L. Mangano, M. Moretti, F. Piccinini, and M. Treccani, "Matching matrix elements and shower evolution for top-quark production in hadronic collisions", *JHEP* **0701** (2007) 013, arXiv:hep-ph/0611129.

[41] C. Oleari, "The POWHEG BOX", *Nuclear Physics B Proceedings Supplements* **205** (August, 2010) 36–41, arXiv:1007.3893.

[42] CMS Collaboration, "MET performance in 8 TeV data", Technical Report CMS-PAS-JME-12-002, CERN, Geneva, 2013.

[43] CMS Collaboration, "Data-Driven Estimation of the Invisible Z Backgrund to the SUSY MET Plus Jets Search", Technical Report CMS-PAS-SUS-08-002, CERN, Geneva, 2008.

[44] J. H. Kuhn, A. Kulesza, S. Pozzorini, and M. Schulze, "Electroweak corrections to hadronic photon production at large transverse momenta", *JHEP* **0603** (2006) 059, arXiv:hep-ph/0508253.

[45] CMS Collaboration, "Measurement of the $pp \to ZZ$ production cross section and constraints on anomalous triple gauge couplings in four-lepton final states at $\sqrt{s}$ =8 TeV", *Phys.Lett.* **B740** (2015) 250–272, doi:10.1016/j.physletb.2014.11.059, arXiv:1406.0113.

[46] CMS Collaboration, "CMS Luminosity Based on Pixel Cluster Counting - Summer 2013 Update", Technical Report CMS-PAS-LUM-13-001, CERN, Geneva, 2013.

[47] A. L. Read, "Presentation of search results: the CLs technique", *Journal of Physics G: Nuclear and Particle Physics* **28** (2002), no. 10, 2693.

[48] A. Kurylov and M. Kamionkowski, "Generalized analysis of weakly interacting massive particle searches", *Phys.Rev.* **D69** (2004) 063503, arXiv:hep-ph/0307185.

[49] J. Hisano, K. Ishiwata, and N. Nagata, "Gluon contribution to the dark matter direct detection", *Phys.Rev.* **D82** (2010) 115007, arXiv:1007.2601.

[50] K. Cheung, C.-T. Lu, P.-Y. Tseng, and T.-C. Yuan, "Collider Constraints on the Dark Matter Interpretation of the CDMS II Results", *ArXiv e-prints* (July, 2013) arXiv:1308.0067.

[51] LUX Collaboration, "The Large Underground Xenon (LUX) Experiment", *Nucl.Instrum.Meth.* **A704** (2013) 111–126, arXiv:1211.3788.

[52] LUX Collaboration, "First results from the LUX dark matter experiment at the Sanford Underground Research Facility", *Phys.Rev.Lett.* **112** (2014), no. 9, 091303, arXiv:1310.8214.

[53] LUX Collaboration, "A Detailed Look at the First Results from the Large Underground Xenon (LUX) Dark Matter Experiment", arXiv:1402.3731.

[54] PICASSO Collaboration, "Constraints on Low-Mass WIMP Interactions on ^{19}F from PICASSO", *Phys.Lett.* **B711** (2012) 153–161, arXiv:1202.1240.

[55] COUPP Collaboration, "First Dark Matter Search Results from a 4-kg CF_3I Bubble Chamber Operated in a Deep Underground Site", *Phys.Rev.* **D86** (2012), no. 5, 052001, arXiv:1204.3094.

[56] M. Felizardo et al., "Final Analysis and Results of the Phase II SIMPLE Dark Matter Search", *Phys.Rev.Lett.* **108** (2012) 201302, arXiv:1106.3014.

[57] Fermi-LAT Collaboration, "Constraining Dark Matter Models from a Combined Analysis of Milky Way Satellites with the Fermi Large Area Telescope", *Phys.Rev.Lett.* **107** (2011) 241302, arXiv:1108.3546.

[58] Fermi-LAT Collaboration, "Observations of Milky Way Dwarf Spheroidal galaxies with the Fermi-LAT detector and constraints on Dark Matter models", *Astrophys.J.* **712** (2010) 147–158, arXiv:1001.4531.

[59] WMAP Collaboration, "The Microwave Anisotropy Probe (MAP) mission", *Astrophys.J.* **583** (2003) 1–23, doi:10.1086/345346, arXiv:astro-ph/0301158.

[60] Planck Collaboration, "The Scientific programme of Planck", arXiv:astro-ph/0604069.

[61] M. Backovic, K. Kong, and M. McCaskey, "MadDM v.1.0: Computation of Dark Matter Relic Abundance Using MadGraph5", *Physics of the Dark Universe* **5-6** (2014) 18–28, doi:10.1016/j.dark.2014.04.001, arXiv:1308.4955.

[62] Planck Collaboration, "Planck 2013 results. XVI. Cosmological parameters", *Astron.Astrophys.* **571** (2014) A16, doi:10.1051/0004-6361/201321591, arXiv:1303.5076.

[63] H. An, X. Ji, and L.-T. Wang, "Light Dark Matter and Z' Dark Force at Colliders", *JHEP* **07** (2012) 182, doi:10.1007/JHEP07(2012)182, arXiv:1202.2894.

[64] S. Malik et al., "Interplay and Characterization of Dark Matter Searches at Colliders and in Direct Detection Experiments", arXiv:1409.4075.

[65] P. Harris, V. V. Khoze, M. Spannowsky, and C. Williams, "Closing up on Dark Sectors at Colliders: from 14 to 100 TeV", arXiv:1509.02904.

[66] F. Calore, I. Cholis, C. McCabe, and C. Weniger, "A Tale of Tails: Dark Matter Interpretations of the Fermi GeV Excess in Light of Background Model Systematics", *Phys. Rev.* **D91** (2015), no. 6, 063003, doi:10.1103/PhysRevD.91.063003, arXiv:1411.4647.

[67] O. Buchmueller, S. A. Malik, C. McCabe, and B. Penning, "Constraining the Fermi-LAT excess with multi-jet plus MET collider searches", arXiv:1505.07826.

[68] M. R. Buckley, D. Feld, and D. Goncalves, "Scalar Simplified Models for Dark Matter", arXiv:1410.6497.